ChemPubSoc Europe

DOI: 10.1002/chem.201500512

CHEMISTRY A European Journal Full Paper

Nanocomposites

Synthesis of Bismuth-Nanoparticle-Enriched Nanoporous Carbon on Graphene for Efficient Electrochemical Analysis of Heavy-Metal Ions

Lin Cui, Jie Wu, and Huangxian Ju*[a]

Abstract: A BiNPs@NPCGS nanocomposite was designed for highly efficient detection of multiple heavy-metal ions by in situ synthesis of bismuth-nanoparticle (BiNP)-enriched nanoporous carbon (NPS) on graphene sheet (GS). The NPCGS was prepared by pyrolysis of zeolitic imidazolate framework-8 (ZIF-8) nanocrystals deposited on graphene oxide and displayed a high surface area of 1251 $m^2 g^{-1}$ and a pore size of 3.4 nm. BiNPs were deposited on NPCGS in situ by chemical reduction of Bi^{3+} with $NaBH_4$. Due to the restrictive effect of the pore/surface structure of NPCGS, the BiNPs were uniform and well dispersed on the NPCGS. The BiNPs@NPCGS showed good conductivity and high effective area, and the presence of BiNPs allowed it to act as an efficient material for anodic-stripping voltammetric detection of heavy-metal ions. Under optimized conditions, the BiNPs@NPCGS-based sensor could simultaneously determine Pb^{2+} and Cd^{2+} with detection limits of 3.2 and 4.1 nM, respectively. Moreover, the proposed sensor could also differentiate Tl^+ from Pb^{2+} and Cd^{2+}. Owing to its advantages of simple preparation, environmental friendliness, high surface area, and fast electron-transfer ability, BiNPs@NPCGS showed promise for practical application in sensing heavy-metal ions.

Introduction

Bismuth-based electrodes have emerged as an effective substitute to mercury-drop and mercury-film electrodes for detection of heavy metals with the advantage of environmental friendliness.[1] These electrodes can be conveniently utilized without removing dissolved oxygen and avoid the interference of hydrogen evolution during stripping analysis.[2] Different Bi precursors, such as Bi oxide, Bi citrate, Bi titanate, Bi aluminate, and Bi zirconate, have been used to develop Bi films for electrochemical measurements.[3] Compared with bismuth films, bismuth nanoparticles (BiNPs) exhibit higher catalytic activity, electroanalytical ability, and signal-to-noise ratio owing to the large surface area, extensive active sites, high surface free energy, and enhanced mass-transfer effect.[4] In addition, due to size-induced quantum confinement effects, BiNPs have tunable electronic properties,[5] which lead to their wide application in the detection of heavy-metal ions.[6]

Normally, BiNPs are combined with functionalized nanomaterials for immobilization on an electrode surface, which enhances the modification amount and improves the stability. Carbon nanomaterials, which have high thermal conductivity, high mechanical strength, excellent electronic-transport ability, and high surface area,[8] are the most extensively used materials in BiNP immobilization. For example, a reduced graphene oxide/BiNPs composite has been proposed for the detection of heavy metals, and detection limits on the $\mu g L^{-1}$ level have been obtained.[9] Nanoporous carbon (NPC) is also extremely attractive in electroanalytical applications due to its low cost, excellent chemical stability, high surface area, and versatile structures.[10] In this work the advantages of BiNPs and NPC were integrated to design a novel nanocomposite, namely, BiNPs@NPCGS, for highly efficient multiple detection of heavy-metal ions. The NPC on graphene sheet (GS) was synthesized by pyrolysis of zeolitic imidazolate framework-8 (ZIF-8) deposited on graphene oxide (Scheme 1).

Metal–organic frameworks (MOFs) are an interesting class of crystalline molecular materials.[11] Their structures are versatile

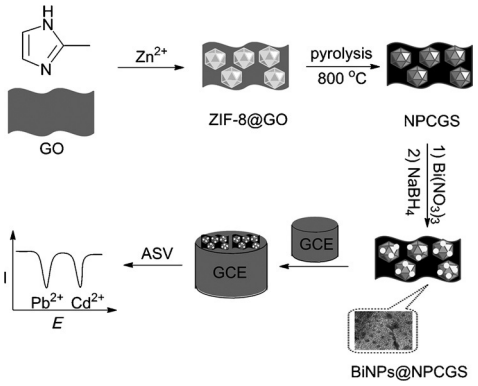

Scheme 1. Schematic synthesis of BiNPs@NPCGS for sensitive electrochemical detection of Pb^{2+} and Cd^{2+}.

[a] L. Cui, Dr. J. Wu, Prof. H. X. Ju
State Key Laboratory of Analytical Chemistry for Life Science
School of Chemistry and Chemical Engineering
Nanjing University
Nanjing 210093 (P. R. China)
Fax: (+86) 25-8359-3593
E-mail: hxju@nju.edu.cn

Supporting information for this article is available on the WWW under http://dx.doi.org/10.1002/chem.201500512.

and controllable by architecture design and pore functionalization. Particularly, their pore size, volume, and functionality are tailorable in a rational manner.[12] As a zeolite-like MOF, ZIF-8 shows a high degree of microporosity and exceptional thermal and chemical stability,[13] and has been used for removal of contaminants and extended environmental applications.[14] In particular, owing to the permanent nanoscale cavities and open channels, ZIF-8 is a good template to synthesize porous carbon directly on carbonization.[15,16] ZIF-8-templated nanoporous materials have been reported to have unexpectedly high surface area, considerable hydrogen-storage capacity, and good electrochemical properties. In addition, N-decorated NPC has also been prepared by using N-enriched ZIF-8 as template and precursor with furfuryl alcohol and NH_4OH as the secondary carbon and nitrogen sources, respectively.[17] This material exhibits remarkable CO_2 adsorption capacity, CO_2/N_2 and CO_2/CH_4 selectivity, and excellent activity for the oxygen reduction reaction.

Herein, NPC was prepared on GS for in situ growth of BiNPs. Due to the π–π interaction between the imidazole ligand and GO, nanosized ZIF-8 could be formed on the surface of GO to produce ZIF-8@GO composite. On carbonization under nitrogen, the obtained nanoporous NPCGS showed good electrical conductivity, high surface area, and large pore volume with a pore size of 2.6 nm. Through in situ deposition of BiNPs on NPCGS, the resulting BiNPs@NPCGS exhibited high effective area and excellent electroanalytical ability to simultaneously detect Pb^{2+} and Cd^{2+} down to the nanomolar level. The synthesized BiNPs@NPCGS was a favorable electrode-modification material and could be applied to design a highly sensitive method for electrochemical assay of heavy-metal ions.

Results and Discussion

Characterization of NPCGS and BiNPs@NPCGS

The crystalline structures of both ZIF-8@GO and NPCGS were analyzed by powder XRD. As shown in Figure 1 A, ZIF-8@GO exhibited a well-recognizable diffraction pattern with reflection peaks (Figure 1 A, curve b) similar to those of the simulated pattern of ZIF-8 (Figure 1 A, curve a), which indicated that ZIF-8@GO retained the nanosized crystals of ZIF-8. In contrast, NPCGS only showed two broad peaks around 24 and 44° (Figure 1 A, curve c). These signals, which correspond to the (002) and (100) planes of turbostratic carbon, indicate the typical graphite structure of NPCGS. In addition, the peak at 44° demonstrated the generation of a high degree of intralayer condensation, which would greatly improve the electrical conductivity of NPCGS.[18] XRD experiments were further performed to characterize the formation of BiNPs@NPCGS (Figure 1 B). The pattern of BiNPs@NPCGS showed obvious peaks of the (012), (104), and (110) planes of the rhombohedral crystal structure of Bi (Figure 1 B, curve b),[19] which confirmed the successful deposition of BiNPs on NPCGS.

Both ZIF-8@GO and NPCGS were further characterized by Raman spectroscopy (Supporting Information, Figure S1). The Raman spectrum of ZIF-8@GO not only showed similar bands

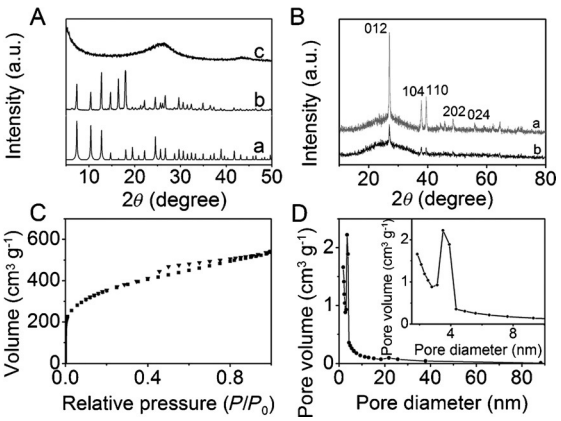

Figure 1. A) XRD patterns of ZIF-8 (a), ZIF-8@GO (b), and NPCGS (c). B) XRD patterns of BiNPs (a) and BiNPs@NPCGS (b). C) N_2 adsorption (▼) and desorption (■) isotherms and D) pore-size distribution of NPCGS. Inset of D): enlarged view of the distribution of small pore diameters.

to ZIF-8 at 168, 686, 1146, and 1458 cm^{-1} corresponding to Zn–N stretching, imidazole ring puckering, C5–N stretching, and methyl bending, respectively,[20] but also showed the typical D and G bands of carbon at 1340 and 1580 cm^{-1}, indicating successful synthesis of ZIF-8@GO. However, only the D and G bands were observed for NPCGS, which suggested complete calcination of ZIF-8 on graphene.

The nitrogen adsorption/desorption isotherm of NPCGS showed a hysteresis loop between the adsorption and desorption branches (Figure 1 C), which implies that it has a nanoporous structure. The surface area of NPCGS determined by the BET method was 1251 $m^2 g^{-1}$, and its porous volume was about 0.81 $cm^3 g^{-1}$. The surface area and porous volume were higher than those of 1067 $m^2 g^{-1}$ and 0.66 $cm^3 g^{-1}$[21] as well as 720 $m^2 g^{-1}$ and 0.26 $m^3 g^{-1}$[22] of reported NPCs. Moreover, the nanopores of NPCGS exhibited a narrow size distribution centered at 3.4 nm (Figure 1 D).

The morphologies of the precursors played a critical role in the preparation of carbon products. Similar to free ZIF-8 (Figure 2 A), a TEM image revealed that the ZIF-8 prepared on GO sheets was nanocrystalline with a mean particle size of 100–120 nm (Figure 2 B). After calcination, the NPCGS exhibited the crumpled and wrinkled flakelike structure of GS along with NPC of high degree of porosity (Figure 2 C), which led to the high specific surface area of NPCGS. After in situ deposition of BiNPs on NPCGS (Figure 2 D), numerous uniformly distributed nanoparticles with a size of about 2 nm were observed on the surface of NPCGS, which indicated the successful formation of BiNPs@NPCGS.

Electrochemical characterization of BiNPs@NPCGS-modified electrodes

The electrochemical features of a BiNPs@NPCGS-modified glassy carbon electrode (BiNPs@NPCGS/GCE) were first investigated in 5 mM $[Fe(CN)_6]^{3-/4-}$ containing 0.1 M KCl (Figure 3 A). Compared with the cyclic voltammograms of bare GCE (Figure 3 A, curve a), BiNPs@RGO/GCE (Figure 3 A, curve b), BiNPs@

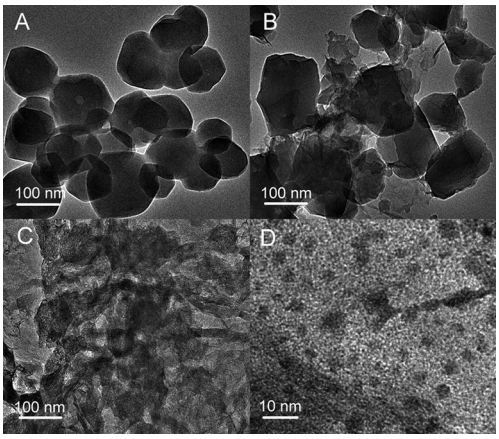

Figure 2. TEM images of A) ZIF-8, B) ZIF-8@GO, C) NPCGS, and D) BiNPs@NPCGS.

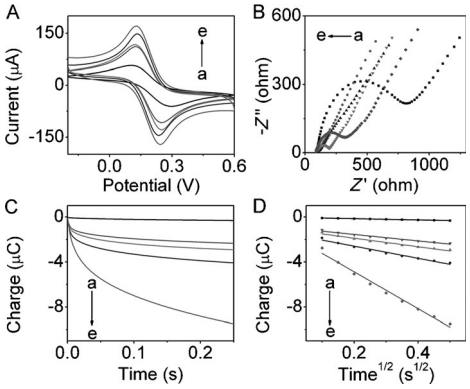

Figure 3. A) Cyclic voltammograms and B) EIS spectra of a) bare GCE, b) BiNPs@RGO/GCE, c) BiNPs@NPC/GCE, d) NPCGS/GCE, and e) BiNPs@NPCGS/GCE in 0.1 M KCl containing 5 mM $[Fe(CN)_6]^{3-/4-}$. Plots of C) Q versus t and D) Q versus $t^{1/2}$ of these electrodes in 0.1 M KCl containing 0.1 mM $K_3[Fe(CN)_6]$.

NPC/GCE (Figure 3A, curve c), and NPCGS/GCE (Figure 3A, curve d), BiNPs@NPCGS/GCE (Figure 3A, curve e) showed enhanced peak currents, and the decrease of ΔE_p to 116 mV (Figure 3A, curve e) from 196 mV (Figure 3A, curve a) suggested faster electron transfer between $[Fe(CN)_6]^{3-/4-}$ and the electrode. Electrochemical impedance spectra (EIS) were also used to evaluate the electron-transfer resistance R_{et} of the modified electrodes (Figure 3B). In a typical EIS, the diameter of the semicircle is equal to R_{et}, which reflects the electron-transfer kinetics of the redox probe at the electrode surface. In comparison with the bare GCE (Figure 3B, curve a), BiNPs@RGO/GCE (Figure 3B, curve b), BiNPs@NPC/GCE (Figure 3B, curve c), and NPCGS/GCE (Figure 3B, curve d), the gradual decrease in R_{et} of BiNPs@NPCGS/GCE (Figure 3B, curve e) confirmed the excellent electric conductivity of BiNPs@NPCGS.

The effective area of BiNPs@NPCGS/GCE was measured by chronocoulometry (Figure 3C) in 0.1 mM $K_3[Fe(CN)_6]$, the diffusion coefficient D of which is 7.6×10^{-6} $cm^2 s^{-1}$,[23] on the basis of Equation (1)[24]

$$Q(t) = \frac{2nFAcD^{1/2}t^{1/2}}{\pi^{1/2}} + Q_{dl} + Q_{ads} \quad (1)$$

where n is the electron-transfer number, A the effective surface area of the working electrode, c the concentration of substrate, D the diffusion coefficient, Q_{dl} the double-layer charge, which could be eliminated by background subtraction, Q_{ads} the Faradaic charge consumed by adsorbed species, and the other symbols have their usual meaning. From Figure 3D, the effective area of BiNPs@NPCGS/GCE was calculated to be 0.546 cm^2, which is much higher than 0.0187 cm^2 of bare GCE, 0.0962 cm^2 of BiNPs@RGO/GCE (curve b), 0.127 cm^2 of BiNPs@NPC/GCE (curve c), and 0.180 cm^2 of NPCGS/GCE (curve d). Such a high effective area of BiNPs@NPCGS/GCE was favorable for designing a highly sensitive platform for sensing heavy-metal ions. This advantage was further confirmed by the square-wave anodic-stripping voltammetric (SWASV) responses of 0.2 μM Pb^{2+} and 0.4 μM Cd^{2+} at different electrodes (Supporting Information, Figure S2). The BiNPs@NPCGS/GCE showed much better defined stripping peaks with larger peak currents than bare GCE, BiNPs@RGO/GCE, BiNPs@NPC/GCE, and NPCGS/GCE, which indicated better absorbability and conductivity of BiNPs@NPCGS toward the target heavy-metal ions.

Optimization of detection conditions

To achieve the maximum sensitivity and precision for tracing heavy-metal ions with BiNPs@NPCGS/GCE, the pH of the detection solution, weight fraction of GO used for material preparation, deposition potential, and time were optimized (Supporting Information, Figure S3). The voltammetric responses of Pb^{2+} and Cd^{2+} showed maxima at pH 5.0, which was selected as the optimal pH for stripping-voltammetric analysis. With increasing weight fraction of GO in the preparation of BiNPs@NPCGS, the SWASV responses of both Pb^{2+} and Cd^{2+} increased and reached maxima at 5.0 wt% GO. Further increases in GO content resulted in a decrease of the SWASV peak current. This phenomenon could be attributed to the relatively low ratio of ZIF-8 to GO, which resulted in less NPC and thus fewer BiNPs on BiNPs@NPCGS. Therefore, 5.0% of GO was selected for the preparation of BiNPs@NPCGS nanocomposite. In addition, when the deposition potential shifted from −0.8 to −1.3 V, the stripping peak currents of both Pb^{2+} and Cd^{2+} increased and reached maxima at −1.0 V. At deposition potentials more negative than −1.0 V, the responses decreased due to competitive generation of H_2. Thus, −1.0 V was chosen as the optimal deposition potential, at which the responses reached the saturated value at a deposition time of 180 s.

Analytical performance

On using BiNPs@NPCGS/GCE to analyze Pb^{2+} and Cd^{2+} simultaneously, two individual and well-defined peaks at approximately −0.6 and −0.8 V were observed (Figure 4A). Because the two peaks were completely separate, detection selectivity and precision of BiNPs@NPCGS/GCE for Pb^{2+} and Cd^{2+} were feasible. The stripping peak currents of both Pb^{2+} and Cd^{2+} in-

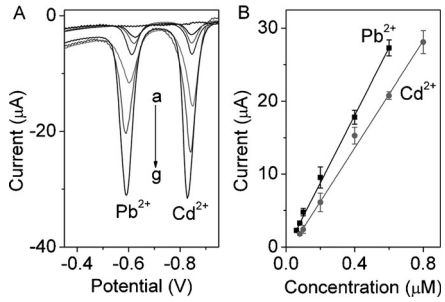

Figure 4. A) SWASV responses of BiNPs@NPCGS/GCE for the simultaneous analysis of Pb^{2+} and Cd^{2+} at 0, 0.06, 0.08, 0.1, 0.2, 0.4, and 0.6 μM for Pb^{2+}, and 0, 0.08, 0.1, 0.2, 0.4, 0.6, and 0.8 μM Cd^{2+} (a–g, respectively). B) Calibration curves for Pb^{2+} and Cd^{2+}.

creased proportionally to increasing concentrations of Pb^{2+} and Cd^{2+}. The corresponding calibration curves for Pb^{2+} and Cd^{2+} showed linear ranges from 0.06 to 0.6 μM and 0.08 to 0.8 μM, respectively (Figure 4B). The linear equations were evaluated as $I/\mu A = -0.44 + 46.27\,C/\mu M$ and $I/\mu A = -1.12 + 36.78\,C/\mu M$ for Pb^{2+} and Cd^{2+}, with correlation coefficients of 0.9970 and 0.9980, respectively. The limits of detection were calculated to be 3.2 nM for Pb^{2+} and 4.1 nM for Cd^{2+}, which are much lower than the respective concentrations of 10[25] and 3 $\mu g\,L^{-1}$[26] in drinking water permitted by the World Health Organization. The detection limit and sensitivity of BiNPs@NPCGS/GCE were greatly superior to those of other stripping-voltammetric detections of Pb^{2+} and Cd^{2+} using electrodes modified with mesoporous silica,[27] carbon nanotubes,[28] Hg film,[29] polyaniline,[30] and bismuth film.[31]

Interference, stability, and repeatability

Mutual interference between heavy-metal ions is a major problem in simultaneous detection. Hence, the mutual interference between Pb^{2+} and Cd^{2+} at BiNPs@NPCGS/GCE was evaluated. On fixing the concentration of Cd^{2+} and increasing the concentration of Pb^{2+}, the peak current of Pb^{2+} increased while that of Cd^{2+} remained the same (Figure 5A). Similarly, when the concentration of Pb^{2+} was fixed and the concentration of Cd^{2+} increased, the peak current of Cd^{2+} increased while the peak current of Pb^{2+} remained the same (Figure 5B). In addition, the calibration plots of peak current versus concentration exhibited good linearity in the ranges of 0.06 to 0.6 μM and 0.08 to 0.6 μM for Pb^{2+} and Cd^{2+}, respectively. The linear equations were evaluated as $I/\mu A = -0.15 + 49.69\,C/\mu M$ and $I/\mu A = -0.71 + 39.60\,C/\mu M$ for Pb^{2+} and Cd^{2+}, with correlation coefficients of 0.9911 and 0.9907, respectively (Figure 5C and D). The detection slopes of both Pb^{2+} and Cd^{2+} were similar to those shown in Figure 4B (49.69 versus 46.27 for Pb^{2+} and 39.60 versus 36.78 for Cd^{2+}), and thus indicated that no mutual interference between Pb^{2+} and Cd^{2+} occurred at BiNPs@NPCGS/GCE. Moreover, the individual SWASV peak of Tl^{+} could also be observed at BiNPs@NPCGS/GCE (Supporting Information, Figure S4), which implies that BiNPs@NPCGS is an efficient material for distinguishing Tl^{+} in a mixture of Pb^{2+} and Cd^{2+}.

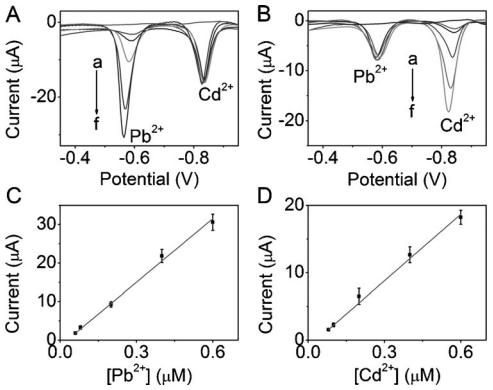

Figure 5. SWASV curves of A) Pb^{2+} at 0, 0.06, 0.08, 0.2, 0.4, and 0.6 μM (from a to f) in the presence of 0.4 μM Cd^{2+} and B) Cd^{2+} at 0, 0.08, 0.1, 0.2, 0.4, and 0.6 μM (from a to f) in the presence of 0.2 μM Pb^{2+} at BiNPs@NPCGS/GCE. C) and D) Corresponding linear calibration plots against [Pb^{2+}] and [Cd^{2+}].

To evaluate the interference of other ions, the effects of various metal ions including Mg^{2+}, Fe^{3+}, Co^{2+}, Ni^{2+}, Zn^{2+}, Hg^{2+}, Mn^{2+}, Cu^{2+}, and Al^{3+} at a concentration of 10 μM on the determination of 0.2 μM Pb^{2+} and 0.4 μM Cd^{2+} was examined at BiNPs@NPCGS/GCE. Except for Cu^{2+} and Hg^{2+} at high concentrations (>1 μM), no remarkable influence was observed, and deviations were less than 5%. Mercury ions could be reduced and form a film on the surface of electrode, which caused Pb^{2+} and Cd^{2+} to be reduced more easily by forming an amalgam.[32] Consequently, the anodic-stripping peak currents increased in the presence of Hg^{2+}. However, the SWASV signals for Pb^{2+} and Cd^{2+} were significantly diminished in the presence of Cu^{2+}, possibly due to the formation of intermetallic compounds.[33] Therefore, ferricyanide was selected to exclude the interference of Cu^{2+}.

The repeatability of BiNPs@NPCGS/GCE was investigated by repetitively determining 0.2 μM Pb^{2+} and 0.4 μM Cd^{2+}. The relative standard deviations (RSDs) of peak currents were 2.6 and 3.0%, respectively ($n = 10$). The response sensitivity was retained to more than 95 and 93% over six weeks. The reproducibility of the electrode preparation was also studied. Six electrodes were prepared from the same batch and evaluated by detecting 0.2 μM Pb^{2+} and 0.4 μM Cd^{2+}. Their RSDs were 2.6 and 2.3%, respectively. The high stability and good reproducibility indicated that the BiNPs@NPCGS-modified electrode was suitable for analysis of real samples.

Real-sample analysis

The feasibility of the detection method using BiNPs@NPCGS/GCE was investigated by detecting Pb^{2+} and Cd^{2+} in natural water samples, including tap water and lake water (from Xuanwu Lake in Nanjing, P. R. China). All samples were filtered through a 0.2 μm membrane prior to detection. These water samples did not show any response of Pb^{2+} and Cd^{2+}, that is, the concentrations of Pb^{2+} and Cd^{2+} were extremely low. The samples were spiked with different concentrations of Pb^{2+} and Cd^{2+} for recovery evaluation (Table 1). The average

Table 1. Determination of Pb^{2+} and Cd^{2+} in water samples with the BiNPs@NPCGS-modified electrode.

Sample		Added [nM]	Result [nM]	Recovery [%]
lake water	Pb^{2+}	100.0	93.2 ± 1.26	93.2
	Cd^{2+}	100.0	101.8 ± 1.31	101.8
tap water	Pb^{2+}	200.0	203.35 ± 1.27	101.7
	Cd^{2+}	200.0	199.24 ± 1.35	99.62

recoveries ranged from 93.2 to 101.8% for three determinations, and this indicated good accuracy of BiNPs@NPCGS/GCE for Pb^{2+} and Cd^{2+} detection in real samples.

Conclusion

A BiNPs@NPCGS nanocomposite with good conductivity and high surface area was synthesized for effective detection of multiple heavy-metal ions. The NPCGS was obtained by calcination of the precursor ZIF-8 deposited on GO, and BiNPs were well-dispersed on NPCGS by in situ reduction. The BiNPs@NPCGS integrated the advantages of BiNPs and NPC for electrochemical analysis of metal ions, and the modified electrode could simultaneously detect Pb^{2+} and Cd^{2+} with high sensitivity and good accuracy. The BiNPs@NPCGS nanocomposite is an excellent electrode-modification material for applications in the fast and convenient determination of heavy-metal ions in environmental systems.

Experimental Section

Materials and reagents

$Zn(NO_3)_2{\cdot}6H_2O$ was purchased from Xilong Chemical Co., Ltd. (P. R. China). 2-Methylimidazole was purchased from Sigma-Aldrich. $CdCl_2{\cdot}2.5H_2O$ was supplied by Alfa Aesar China Ltd. (P. R. China). $Pb(NO_3)_2$ and other metal salts were purchased from Nanjing Chemistry Agent Co., Ltd. (P. R. China). GO and reduced GO (RGO) were purchased from XFNANO Materials Tech Co., Ltd. (Nanjing, P. R. China). 0.1 M acetate buffer solutions with different pHs were prepared by mixing stock solutions of 0.1 M sodium acetate and acetic acid. Other reagents were of analytical grade and used as received. Ultrapure water obtained from a Millipore water purification system (≥18 MΩ cm, Milli-Q, Millipore) was used in all assays.

Apparatus

All electrochemical experiments were performed on a CHI660D electrochemical workstation (CH Instruments Inc., U.S.A.) with a conventional three-electrode cell, in which bare or modified glassy carbon electrode (GCE, $d = 3$ mm), SCE, and platinum wire served as the working, reference, and auxiliary electrodes, respectively. EIS analysis was performed in 5 mM $[Fe(CN)_6]^{3-/4-}$ containing 0.1 M KCl. TEM images were recorded on a JEM 2100 high-resolution transmission electron microscope (JEOL, Japan). XRD patterns were measured on Rigaku Dmax 2200 X-ray diffractometer with $Cu_{K\alpha}$ radiation ($\lambda = 1.5416$ A). Nitrogen adsorption/desorption isotherms and pore size distributions were measured at 77 K by using a Micrometeritics ASAP 2020 system. Surface-enhanced Raman scattering measurements were performed with a Renishaw in Via-Reflex Raman microscope system (Renishaw, U.K.).

Preparation of NPCGS and BiNPs@NPCGS

The ZIF-8 nanocrystals were prepared according to a previous report.[13a] $Zn(NO_3)_2{\cdot}6H_2O$ (1.17 g, 3.95 mmol) in 8 mL of ultrapure water was added to a solution of 2-methylimidazole (22.7 g, 276.5 mmol) in methanol (80 mL) with stirring at room temperature. After stirring for about 5 min, the ZIF-8 nanocrystals were collected by centrifugation, washed with ultrapure water several times, and dried at 60 °C. For the preparation of ZIF-8@GO, 80 mL GO solutions in methanol with different weight fractions compared to Zn^{II} were prepared and mixed with 2-methylimidazole (22.7 g). After stirring for 30 min, a solution of $Zn(NO_3)_2{\cdot}6H_2O$ (1.17 g in 8 mL) was added to the solution. The mixture was stirred for 1 h at room temperature, and then the product was collected by centrifugation, washed several times with ultrapure water, and dried at 60 °C.

ZIF-8@GO was heated to 800 °C at a rate of 5 °C min^{-1} and then pyrolyzed at 800 °C for 2 h under N_2. After cooling to room temperature, the resultant black powder was collected and stirred in 10 wt% HCl solution for 24 h. Then, the product was collected by centrifugation, rinsed with ultrapure water, and dried at 60 °C overnight to obtain NPCGS.

NPCGS (2.0 mg) was dispersed in 5 mL of ethylene glycol (EG) and the dispersion ultrasonicated for 1 h. After dissolving 4.85 mg of sodium citrate in the dispersion, 5 mL of $Bi(NO_3)_3{\cdot}5H_2O$ (8.15 mg) in EG was added and the mixture stirred for 12 h. Then 0.5 mL of 0.1 M $NaBH_4$ was added to the mixture. After shaking for 1 h, the as-synthesized solid products were separated by centrifugation, washed thoroughly with ultrapure water and absolute ethanol to remove any impurities, and dried in a vacuum oven at 50 °C for 24 h to obtain BiNPs@NPCGS nanocomposite. The BiNPs, BiNPs@NPC, and BiNPs@RGO were prepared by similar procedures.

Electrochemical detection of Pb^{2+} and Cd^{2+}

Firstly, the bare GCE was polished with 0.3 and 0.05 μm alumina slurry on microcloth pads, successively sonicated with pure water and ethanol for 3 min, and dried with nitrogen. 5 μL of 1 mg mL^{-1} BiNPs@NPCGS in ethanol was then dropped onto the electrode surface. After the solvent was evaporated, the electrode was thoroughly rinsed with deionized water, and dried in a nitrogen stream. The NPCGS-, BiNPs@GS-, and BiNPs@NPC-modified GC electrodes were prepared by similar procedures. SWASV was used for the detection of Pb^{2+} and Cd^{2+} with a deposition potential of −1.0 V for 180 s in 0.1 M acetate buffer (pH 5.0). The anodic stripping of electrodeposited metal was performed in the potential range of −0.95 to −0.35 V with the following parameters: frequency, 15 Hz; amplitude, 25 mV; increment potential, 4 mV.

Acknowledgements

We gratefully acknowledge the National Special Project for Key Scientific Apparatus Development (2012YQ170000302), National Natural Science Foundation of China (21135002 and 21361162002), and Priority development areas of The National Research Foundation for the Doctoral Program of Higher Education of China (20130091130005).

Keywords: bismuth · electrochemistry · nanostructures · voltammetry · zeolite analogues

[1] J. Wang, J. M. Lu, S. B. Hocevar, P. A. M. Farias, *Anal. Chem.* **2000**, *72*, 3218 – 3222.
[2] a) M. A. Baldo, S. Daniele, *Anal. Lett.* **2005**, *37*, 995 – 1011; b) H. J. Kim, D. W. Son, J. M. Park, D. Y. Hwang, C. Y. Mo, S. W. Park, G. Kim, J. B. Eun, *Food Sci. Biotechnol.* **2010**, *19*, 1211 – 1217.
[3] N. Serrano, A. Alberich, J. M. Diaz-Cruz, C. Arino, M. Esteban, *TrAC Trends Anal. Chem.* **2013**, *46*, 15 – 29.
[4] K. E. Toghill, R. G. Compton, *Electroanalysis* **2010**, *22*, 1947 – 1956.
[5] F. D. Wang, R. Tang, H. Yu, P. C. Gibbons, W. E. Buhro, *Chem. Mater.* **2008**, *20*, 3656 – 3662.
[6] a) P. Rattanarat, W. Dungchai, D. M. Cate, J. Volckens, O. Chailapakul, C. S. Henry, *Anal. Chem.* **2014**, *86*, 3555 – 3562; b) K. E. Toghill, G. G. Wildgoose, A. Moshar, C. Mulcahy, R. G. Compton, *Electroanalysis* **2008**, *20*, 1731 – 1737.
[7] G. J. Lee, C. K. Kim, M. K. Lee, C. K. Rhee, *Talanta* **2010**, *83*, 682 – 685.
[8] K. S. Novoselov, A. K. Geim, S. V. Morozov, D. Jiang, M. I. Katsnelson, I. V. Grigorieva, S. V. Dubonos, A. A. Firsov, *Nature* **2005**, *438*, 197 – 200.
[9] P. K. Sahoo, B. Panigrahy, S. Sahoo, A. K. Satpati, D. Li, D. Bahadur, *Biosens. Bioelectron.* **2013**, *43*, 293 – 296.
[10] a) G. Aragay, J. Pons, A. Merkoci, *J. Mater. Chem.* **2011**, *21*, 4326 – 4331; b) J. S. Huang, B. G. Sumpter, V. Meunier, *Chem. Eur. J.* **2008**, *14*, 6614 – 6626.
[11] a) H. Furukawa, F. Gandara, Y. B. Zhang, J. C. Jiang, W. L. Queen, M. R. Hudson, O. M. Yaghi, *J. Am. Chem. Soc.* **2014**, *136*, 4369 – 4381; b) S. L. Li, Q. Xu, *Energy Environ. Sci.* **2013**, *6*, 1656 – 1683.
[12] a) H. H. Wu, R. S. Reali, D. A. Smith, M. C. Trachtenberg, J. Li, *Chem. Eur. J.* **2010**, *16*, 13951 – 13954; b) C. Wang, D. M. Liu, W. B. Lin, *J. Am. Chem. Soc.* **2013**, *135*, 13222 – 13234; c) A. A. Talin, A. Centrone, A. C. Ford, M. E. Foster, V. Stavila, P. Haney, R. A. Kinney, V. Szalai, F. E. Gabaly, H. P. Yoon, F. Léonard, M. D. Allendorf, *Science* **2014**, *343*, 66 – 69.
[13] a) Y. C. Pan, Y. Y. Liu, G. F. Zeng, L. Zhao, Z. P. Lai, *Chem. Commun.* **2011**, *47*, 2071 – 2073; b) Y. Q. Tian, Y. M. Zhao, Z. X. Chen, G. N. Zhang, L. H. Weng, D. Y. Zhao, *Chem. Eur. J.* **2007**, *13*, 4146 – 4154; c) J. Cravillon, S. Muenzer, S. J. Lohmeier, A. Feldhoff, K. Huber, M. Wiebcke, *Chem. Mater.* **2009**, *21*, 1410 – 1412.
[14] Y. H. Wang, S. G. Jin, Q. Y. Wang, G. H. Lu, J. J. Jiang, D. R. Zhu, *J. Chromatogr. A* **2013**, *1291*, 27 – 32.
[15] a) S. J. Yang, S. Nam, T. Kim, J. H. Im, H. Jung, J. H. Kang, S. Wi, B. Park, C. R. Park, *J. Am. Chem. Soc.* **2013**, *135*, 7394 – 7397; b) M. Hu, J. Reboul, S. Furukawa, N. L. Torad, Q. M. Ji, P. Srinivasu, K. Ariga, S. Kitagawa, Y. Yamauchi, *J. Am. Chem. Soc.* **2012**, *134*, 2864 – 2867; c) T. Palaniselvam, B. P. Biswal, R. Banerjee, S. Kurungot, *Chem. Eur. J.* **2013**, *19*, 9335 – 9342; d) H. J. Lee, S. Choi, M. Oh, *Chem. Commun.* **2014**, *50*, 4492 – 4495.
[16] H. L. Jiang, B. Liu, Y. Q. Lan, K. Kuratani, T. Akita, H. Shioyama, F. Q. Zong, Q. Xu, *J. Am. Chem. Soc.* **2011**, *133*, 11854 – 11857.
[17] A. Aijaz, N. Fujiwara, Q. Xu, *J. Am. Chem. Soc.* **2014**, *136*, 6790 – 6793.
[18] J. P. Paraknowitsch, J. Zhang, D. S. Su, A. Thomas, M. Antonietti, *Adv. Mater.* **2010**, *22*, 87 – 92.
[19] E. E. Foos, R. M. Stroud, A. D. Berry, A. W. Snow, J. P. Armistead, *J. Am. Chem. Soc.* **2000**, *122*, 7114 – 7115.
[20] G. Kumari, K. Jayaramulu, T. K. Maji, C. Narayana, *J. Phys. Chem. A* **2013**, *117*, 11006 – 11012.
[21] P. H. Ling, Q. Hao, J. P. Lei, H. X. Ju, *J. Mater. Chem. B* **2015**, *3*, 1335 – 1341.
[22] W. Chaikittisilp, M. Hu, H. J. Wang, H. S. Huang, T. Fujita, K. C. W. Wu, L. C. Chen, Y. Yamauchi, K. Ariga, *Chem. Commun.* **2012**, *48*, 7259 – 7261.
[23] R. N. Adams, *Electrochemistry at Solid Electrodes*, Marcel Dekker, Inc., New York, **1969**, pp. 222 – 225.
[24] F. C. Anson, *Anal. Chem.* **1964**, *36*, 932 – 934.
[25] P. Chooto, P. Wararatananurak, C. Innuphat, *ScienceAsia* **2010**, *36*, 150 – 156.
[26] S. Cerutti, M. F. Silva, J. A. Gasquez, R. A. Olsina, L. D. Martinez, *Spectrochim. Acta Part B* **2003**, *58*, 43 – 50.
[27] P. H. Zhang, S. Y. Dong, G. Z. Gu, T. L. Huang, *Bull. Korean Chem. Soc.* **2010**, *31*, 2949 – 2954.
[28] K. B. Wu, S. S. Hu, J. J. Fei, W. Bai, *Anal. Chim. Acta* **2003**, *489*, 215 – 221.
[29] R. Güell, G. Aragay, C. Fontas, E. Antico, A. Merkoci, *Anal. Chim. Acta* **2008**, *627*, 219 – 224.
[30] Z. M. Wang, E. J. Liu, X. Zhao, *Thin Solid Films* **2011**, *519*, 5285 – 5289.
[31] W. Siriangkhawut, S. Pencharee, K. Grudpan, J. Jakmunee, *Talanta* **2009**, *79*, 1118 – 1124.
[32] J. Schiewe, K. B. Oldham, J. C. Myland, A. M. Bond, V. A. Vicente-Beckett, S. Fletcher, *Anal. Chem.* **1997**, *69*, 2673 – 2681.
[33] R. J. Grim, *J. Phys. Chem.* **1942**, *46*, 464 – 469.

Received: February 7, 2015
Published online on June 30, 2015

